Modeling the Flow of a Bautista-Manero Fluid in Porous Media

Taha Sochi[*]

2009

[*]University College London - Department of Physics & Astronomy - Gower Street - London.
Email: t.sochi@ucl.ac.uk.

Abstract

In this article, the extensional flow and viscosity and the converging-diverging geometry were examined as the basis of the peculiar viscoelastic behavior in porous media. The modified Bautista-Manero model, which successfully describes shear-thinning, elasticity and thixotropic time-dependency, was used for modeling the flow of viscoelastic materials which also show thixotropic attributes. An algorithm, originally proposed by Philippe Tardy, that employs this model to simulate steady-state time-dependent flow was implemented in a non-Newtonian flow simulation code using pore-scale modeling and the initial results were analyzed. The findings are encouraging for further future development.

Contents

List of Figures

List of Tables

1   Introduction

Non-Newtonian fluids are commonly divided into three broad groups [1, 2]:

1. Time-independent: those fluids for which the strain rate at a given point is solely dependent upon the instantaneous stress at that point.

2. Viscoelastic: those fluids that show partial elastic recovery upon the removal of a deforming stress.

3. Time-dependent: those fluids for which the strain rate is a function of both the magnitude and the duration of stress and possibly of the time lapse between consecutive applications of stress.

A large number of models have been proposed in the literature to model all types of non-Newtonian fluids under various flow conditions. Most these models are basically empirical in nature and arising from curve-fitting exercises [3]. In this article, we investigate a non-Newtonian rheological model (namely Bautista-Manero model) that can be used to describe viscoelastic behavior with thixotropic attributes in the context of pore-scale modeling of non-Newtonian flow through porous media.

2 Viscoelastic Fluids

Viscoelastic substances exhibit a dual nature of behavior by showing signs of both viscous fluids and elastic solids. In its most simple form, viscoelasticity can be modeled by combining Newton's law for viscous fluids (stress $\propto$ rate of strain) with Hook's law for elastic solids (stress $\propto$ strain), as given by the original Maxwell model and extended by the Convected Maxwell models for the nonlinear viscoelastic fluids. Although this idealization predicts several basic viscoelastic phenomena, it does so only qualitatively [4].

Polymeric fluids often show strong viscoelastic effects, which can include shear-thinning, extension thickening, viscoelastic normal stresses, and time-dependent rheology phenomena. The equations describing the flow of viscoelastic fluids consist of the basic laws of continuum mechanics and the rheological equation of state, or constitutive equation, describing a particular fluid and relates the viscoelastic stress to the deformation history. The quest is to derive a model that is as simple as possible, involving the minimum number of variables and parameters, and yet having the capability to predict the viscoelastic behavior in complex flows [5].

No theory is yet available that can adequately describe all of the observed viscoelastic phenomena in a variety of flows. However, many differential and integral viscoelastic constitutive models have been proposed in the literature. What is common to all these is the presence of at least one characteristic time parameter to account for the fluid memory, that is the stress at the present time depends upon the strain or rate-of-strain for all past times, but with an exponentially fading memory [6, 7, 8, 9, 10].

The behavior of viscoelastic fluids is drastically different from that of Newtonian and inelastic non-Newtonian fluids. This includes the presence of normal stresses in shear flows, sensitivity to deformation type, and memory effects such as stress relaxation and time-dependent viscosity. These features underlie the observed peculiar viscoelastic phenomena such as rod-climbing (Weissenberg effect), die swell and open-channel siphon [4, 11]. Most viscoelastic fluids exhibit shear-thinning and an elongational viscosity that is both strain and extensional strain rate dependent, in contrast to Newtonian fluids where the elongational viscosity is constant [11].

The behavior of viscoelastic fluids at any time is dependent on their recent deformation history, that is they possess a fading memory of their past. Indeed a material that has no memory cannot be elastic, since it has no way of remem-

bering its original shape. Consequently, an ideal viscoelastic fluid should behave as an elastic solid in sufficiently rapid deformations and as a Newtonian liquid in sufficiently slow deformations. The justification is that the larger the strain rate, the more strain is imposed on the sample within the memory span of the fluid [4, 11, 12].

Many materials are viscoelastic but at different time scales that may not be reached. Dependent on the time scale of the flow, viscoelastic materials mainly show viscous or elastic behavior. The particular response of a sample in a given experiment depends on the time scale of the experiment in relation to a natural time of the material. Thus, if the experiment is relatively slow, the sample will appear to be viscous rather than elastic, whereas, if the experiment is relatively fast, it will appear to be elastic rather than viscous. At intermediate time scales mixed viscoelastic response is observed. Therefore the concept of a natural time of a material is important in characterizing the material as viscous or elastic. The ratio between the material time scale and the time scale of the flow is indicated by a non-dimensional number: the Deborah or the Weissenberg number [3, 13].

A common feature of viscoelastic fluids is stress relaxation after a sudden shearing displacement where stress overshoots to a maximum then starts decreasing exponentially and eventually settles to a steady state value. This phenomenon also takes place on cessation of steady shear flow where stress decays over a finite measurable length of time. This reveals that viscoelastic fluids are able to store and release energy in contrast to inelastic fluids which react instantaneously to the imposed deformation [4, 10, 12].

A defining characteristic of viscoelastic materials associated with stress relaxation is the relaxation time which may be defined as the time required for the shear stress in a simple shear flow to return to zero under constant strain condition. Hence for a Hookean elastic solid the relaxation time is infinite, while for a Newtonian fluid the relaxation of the stress is immediate and the relaxation time is zero. Relaxation times which are infinite or zero are never realized in reality as they correspond to the mathematical idealization of Hookean elastic solids and Newtonian liquids. In practice, stress relaxation after the imposition of constant strain condition takes place over some finite non-zero time interval [8].

The complexity of viscoelasticity is phenomenal and the subject is notorious for being extremely difficult and challenging. The constitutive equations for viscoelastic fluids are much too complex to be treated in a general manner. Further

complications arise from the confusion created by the presence of other phenomena such as wall effects and polymer-wall interactions, and these appear to be system specific. Therefore, it is doubtful that a general fluid model capable of predicting all the flow responses of viscoelastic system with enough mathematical simplicity or tractability can emerge in the foreseeable future [10, 14, 15]. Understandably, despite the huge amount of literature composed in the last few decades on this subject, almost all these studies have investigated very simple cases in which substantial simplifications have been made using basic viscoelastic models.

In the last few decades, a general consensus has emerged that in the flow of viscoelastic fluids through porous media elastic effects should arise, though their precise nature is unknown or controversial. In porous media, viscoelastic effects can be important in certain cases. When they are, the actual pressure gradient will exceed the purely viscous gradient beyond a critical flow rate, as observed by several investigators. The normal stresses of high molecular polymer solutions can explain in part the high flow resistances encountered during viscoelastic flow through porous media. It is argued that the very high normal stress differences and Trouton ratios (defined as extensional to shear viscosity) associated with polymeric fluids will produce increasing values of apparent viscosity when flow channels in the porous medium are of rapidly changing cross section.

Important aspects of non-Newtonian flow in general and viscoelastic flow in particular through porous media are still presenting serious challenge for modeling and quantification. There are intrinsic difficulties of characterizing non-Newtonian effects in the flow of polymer solutions and the complexities of the local geometry of the porous medium which give rise to a complex and pore-space-dependent flow field in which shear and extension coexist in various proportions that cannot be quantified. Flows through porous media cannot be classified as pure shear flows as the converging-diverging passages impose a predominantly extensional flow fields especially at high flow rates. Moreover, the extension viscosity of many non-Newtonian fluids increases dramatically with the extension rate. As a consequence, the relationship between the pressure drop and flow rate very often do not follow the observed Newtonian and inelastic non-Newtonian trend. Further complication arises from the fact that for complex fluids the stress depends not only on whether the flow is a shearing, extensional, or mixed type, but also on the whole history of the velocity gradient [5, 16, 17, 18, 19, 20].

3   Important Aspects for Viscoelastic Flow in Porous Media

Strong experimental evidence indicates that the flow of viscoelastic fluids through packed beds can exhibit rapid increases in the pressure drop, or an increase in the apparent viscosity, above that expected for a comparable purely viscous fluid. This increase has been attributed to the extensional nature of the flow field in the pores caused by the successive expansions and contractions that a fluid element experiences as it traverses the pore space. Even though the flow field at pore level is not an ideal extensional flow due to the presence of shear and rotation, the increase in flow resistance is referred to as an extension thickening effect [19, 21, 22, 23].

There are two major interrelated aspects that have strong impact on the flow through porous media. These are extensional flow and converging-diverging geometry.

3.1   Extensional Flow

One complexity in the flow in general and through porous media in particular usually arises from the coexistence of shear and extensional components; sometimes with the added complication of inertia. Pure shear or elongational flow is very much the exception in practical situations, especially in the flow through porous media. By far the most common situation is for mixed flow to occur where deformation rates have components parallel and perpendicular to the principal flow direction. In such flows, the elongational components may be associated with the converging-diverging flow paths [3, 24].

A general consensus has emerged recently that the flow through packed beds has a substantial extensional component and typical polymer solutions exhibit strain hardening in extension, which is mainly responsible for the reported dramatic increases in pressure drop. Thus in principle the shear viscosity alone is inadequate to explain the observed excessive pressure gradients. It is therefore essential to know the relative importance of elastic and viscous effects or equivalently the relationship between normal and shear stresses for different shear rates [10, 15, 25].

Elongational flow is fundamentally different from shear, the material property characterizing the flow is not the viscosity, but the elongational viscosity. The behavior of the extensional viscosity function is very often qualitatively different

from that of the shear viscosity function. For example, highly elastic polymer solutions that possess a viscosity which decreases monotonically in shear often exhibit an extensional viscosity that increases dramatically with strain rate. Thus, while the shear viscosity is shear-thinning the extensional viscosity is extension thickening [3, 5, 13].

3.2 Converging-Diverging Geometry

An important aspect that characterizes the flow in porous media and makes it distinct from bulk is the presence of converging-diverging flow paths. This geometric factor significantly affects the flow and accentuate elastic responses. Several arguments have been presented in the literature to explain the effect of converging-diverging geometry on the flow behavior. Despite this diversity, there is a general consensus that in porous media the converging-diverging nature of the flow paths brings out both the extensional and shear properties of the fluid. The principal mode of deformation to which a material element is subjected as the flow converges into a constriction involves both a shearing of the material element and a stretching or elongation in the direction of flow, while in the diverging portion the flow involves both shearing and compression. The actual channel geometry determines the ratio of shearing to extensional contributions. In many realistic situations involving viscoelastic flows the extensional contribution is the most important of the two modes. As porous media flow involves elongational flow components, the coil-stretch phenomenon can also take place. Consequently, a suitable model pore geometry is one having converging and diverging sections which can reproduce the elongational nature of the flow, a feature that is not exhibited by straight capillary tubes [10, 16, 23, 26, 27].

For long time, the straight capillary tube has been the conventional model for porous media and packed beds. Despite the general success of this model with the Newtonian and inelastic non-Newtonian flow, its failure with elastic flow was remarkable. To redress the flaws of this model, the undulating tube and converging-diverging channel were proposed in order to include the elastic character of the flow. Various corrugated tube models with different simple geometries have been used as a first step to model the effect of converging-diverging geometry on the flow of viscoelastic fluids in porous media (e.g. [16, 22, 28]). Those geometries include conically shaped sections, sinusoidal corrugation and abrupt expansions and contractions. Similarly, a bundle of converging-diverging tubes forms a better

model for a porous medium in viscoelastic flow than the normally used bundle of straight capillary tubes, as the presence of diameter variations makes it possible to account for elongational contributions.

Many investigators have attempted to capture the role of the successive converging-diverging character of packed bed flow by numerically solving the flow equations in conduits of periodically varying cross sections. Different opinions on the success of these models can be found in the literature. Examples include [10, 15, 23, 26, 29, 30]. With regards to modeling viscoelastic flow in regular or random networks of converging-diverging capillaries, very little work has been done.

4 Modeling the Flow in Porous Media

The basic equations describing the flow of fluids consist of the basic laws of continuum mechanics which are the conservation principles of mass, energy and linear and angular momentum. These governing equations indicate how the mass, energy and momentum of the fluid change with position and time. The basic equations have to be supplemented by a suitable rheological equation of state, or constitutive equation describing a particular fluid, which is a differential or integral mathematical relationship that relates the extra stress tensor to the rate-of-strain tensor in general flow condition and closes the set of governing equations. One then solves the constitutive model together with the conservation laws using a suitable method to predict velocity and stress fields of the flows [7, 12, 25, 31, 32, 33].

The mathematical description of the flow in porous media is extremely complex task and involves many approximations. So far, no analytical fluid mechanics solution to the flow through porous media has been found. Furthermore, such a solution is apparently out of reach for the foreseeable future. Therefore, to investigate the flow through porous media other methodologies have been developed, the main ones are the macroscopic continuum approach and the pore-scale numerical approach.

The widely used continuum models represent a simplified macroscopic approach in which the porous medium is treated as a continuum. All the complexities and fine details of the microscopic pore structure are absorbed into bulk terms like permeability that reflect average properties of the medium. Semi-empirical equations such as Darcy's law, Blake-Kozeny-Carman or Ergun equation fall into this category. Several continuum models are based in their derivation on the capillary bundle concept. The advantage of the continuum method is that it is simple and easy to implement with no computational cost. The disadvantage is that it does not account for the detailed physics at the pore level. One consequence of this is that in most cases it can only deal with steady-state situations with no time-dependent transient effects.

In the numerical approach, a detailed description of the porous medium at pore-scale level is adopted and the relevant physics of flow at this level is applied. To find the solution, numerical methods, such as finite volume and finite difference, usually in conjunction with computational implementation are used. The advantage of the numerical method is that it is the most direct approach to describe the physical

situation and the closest to full analytical solution. It is also capable, in principle at least, to deal with time-dependent transient situations. The disadvantage is that it requires a detailed pore space description. Moreover, it is usually very complex and hard to implement and has a huge computational cost with serious convergence difficulties. Due to these complexities, the flow processes and porous media that are currently within the reach of numerical investigation are the most simple ones.

Pore-scale network modeling is a relatively novel method developed to deal with flow through porous media. It can be seen as a compromise between these two extreme approaches as it partly accounts for the physics and void space description at the pore level with reasonable and generally affordable computational cost. Network modeling can be used to describe a wide range of properties from capillary pressure characteristics to interfacial area and mass transfer coefficients. The void space is described as a network of pores connected by throats. The pores and throats are assigned some idealized geometry, and rules which determine the transport properties in these elements are incorporated in the network to compute effective transport properties on a mesoscopic scale. The appropriate pore-scale physics combined with a geologically representative description of the pore space gives models that can successfully predict average behavior [34, 35].

In our investigation to the flow of Bautista-Manero fluids in porous media we use network modeling. Our model uses three-dimensional networks built from a topologically-equivalent three-dimensional voxel image of the pore space with the pore sizes, shapes and connectivity reflecting the real medium. Pores and throats are modeled as having triangular, square or circular cross-section by assigning a shape factor which is the ratio of the area to the perimeter squared and obtained from the pore space image. Most of the network elements are not circular. To account for the non-circularity when calculating the volumetric flow rate analytically or numerically for a cylindrical capillary, an equivalent radius R_{eq} is defined:

$$R_{eq} = \left(\frac{8G}{\pi}\right)^{1/4} \tag{1}$$

where the geometric conductance, G, is obtained empirically from numerical simulation. Two networks obtained from Statoil and representing two different porous media have been used: a sand pack and a Berea sandstone. These networks are constructed by Øren and coworkers [36, 37] from voxel images generated by simulating the geological processes by which the porous medium was formed. The

physical and statistical properties of the networks are given in [38].

Assuming a laminar, isothermal and incompressible flow at low Reynolds number, the only equations that need to be considered are the constitutive equation for the particular fluid and the conservation of volume as an expression for the conservation of mass. Because initially the pressure drop in each network element is not known, an iterative method is used. This starts by assigning an effective viscosity to each network element. The effective viscosity is defined as that viscosity which makes Poiseulle's equation fit any set of laminar flow conditions for time-independent fluids [1]. By invoking the conservation of volume for incompressible fluid, the pressure field across the entire network is solved using a numerical solver [39]. Knowing the pressure drops, the effective viscosity of each element is updated using the expression for the flow rate with a pseudo-Poiseuille definition. The pressure field is then recomputed using the updated viscosities and the iteration continues until convergence is achieved when a specified error tolerance in total flow rate between two consecutive iteration cycles is reached. Finally, the total volumetric flow rate and the apparent viscosity in porous media, defined as the viscosity calculated from the Darcy's law, are obtained.

With regards to modeling the flow in porous media of complex fluids which have time dependency due to thixotropic or elastic nature, there are three major difficulties :

- The difficulty of tracking the fluid elements in the pores and throats and identifying their deformation history, as the path followed by these elements is random and can have several unpredictable outcomes.

- The mixing of fluid elements with various deformation history in the individual pores and throats. As a result, the viscosity is not a well-defined property of the fluid in the pores and throats.

- The change of viscosity along the streamline since the deformation history is constantly changing over the path of each fluid element.

In the current work, we deal only with one case of steady-state viscoelastic flow, and hence we did not consider these complications in depth. Consequently, the tracking of fluid elements or flow history in the network and other dynamic aspects are not implemented in the non-Newtonian code. However, time-dependent effects in steady-state conditions are accounted for in the Tardy algorithm which is implemented in the code and will be presented in detail in § (5.1).

In our modeling approach, to solve the pressure field across a network of n nodes we write n equations in n unknowns which are the pressure values at the nodes. The essence of these equations is the continuity of flow of incompressible fluid at each node in the absence of source and sink. We solve this set of equations subject to the boundary conditions which are the pressures at the inlet and outlet. This unique solution is 'consistent' and 'stable' as it is the only mathematically acceptable solution to the problem, and, assuming the modeling process and the mathematical technicalities are correct, should mimic the unique physical reality of the pressure field in the porous medium.

5   Bautista-Manero Model

This is a relatively simple model that combines the Oldroyd-B constitutive equation for viscoelasticity and the Fredrickson's kinetic equation for flow-induced structural changes usually associated with thixotropy. The model requires six parameters that have physical significance and can be estimated from rheological measurements. These parameters are the low and high shear rate viscosities, the elastic modulus, the relaxation time, and two other constants describing the build up and break down of viscosity.

The Oldroyd-B model is a simplification of the more elaborate and rarely used Oldroyd 8-constant model which also contains the upper convected, the lower convected, and the corotational Maxwell equations as special cases. Oldroyd-B is the second simplest nonlinear viscoelastic model and is apparently the most popular in viscoelastic flow modeling and simulation. It is the nonlinear equivalent of the linear Jeffreys model, and hence it takes account of frame invariance in the nonlinear regime. Consequently, in the linear viscoelastic regime the Oldroyd-B model reduces to the linear Jeffreys model. The Oldroyd-B model can be obtained by replacing the partial time derivatives in the differential form of the Jeffreys model with the upper convected time derivatives [12]

$$\boldsymbol{\tau} + \lambda_1 \overset{\triangledown}{\boldsymbol{\tau}} = \mu_o \left(\dot{\boldsymbol{\gamma}} + \lambda_2 \overset{\triangledown}{\dot{\boldsymbol{\gamma}}} \right) \tag{2}$$

where $\boldsymbol{\tau}$ is the extra stress tensor, λ_1 is the relaxation time, λ_2 is the retardation time, μ_o is the low-shear viscosity, $\dot{\boldsymbol{\gamma}}$ is the rate-of-strain tensor, and $\overset{\triangledown}{\boldsymbol{\tau}}$ is the upper convected time derivative of the stress tensor:

$$\overset{\triangledown}{\boldsymbol{\tau}} = \frac{\partial \boldsymbol{\tau}}{\partial t} + \mathbf{v} \cdot \nabla \boldsymbol{\tau} - (\nabla \mathbf{v})^T \cdot \boldsymbol{\tau} - \boldsymbol{\tau} \cdot \nabla \mathbf{v} \tag{3}$$

where t is time, $\mathbf{v} = (v_x, v_y, v_z)$ is the fluid velocity vector, $(\cdot)^T$ is the transpose of the tensor and $\nabla \mathbf{v}$ is the fluid velocity gradient tensor defined by

$$\nabla \mathbf{v} = \begin{pmatrix} \frac{\partial v_x}{\partial x} & \frac{\partial v_x}{\partial y} & \frac{\partial v_x}{\partial z} \\ \frac{\partial v_y}{\partial x} & \frac{\partial v_y}{\partial y} & \frac{\partial v_y}{\partial z} \\ \frac{\partial v_z}{\partial x} & \frac{\partial v_z}{\partial y} & \frac{\partial v_z}{\partial z} \end{pmatrix} \tag{4}$$

Similarly, $\overset{\triangledown}{\dot{\boldsymbol{\gamma}}}$ is the upper convected time derivative of the rate-of-strain tensor

given by:

$$\overset{\triangledown}{\dot{\boldsymbol{\gamma}}} = \frac{\partial \dot{\boldsymbol{\gamma}}}{\partial t} + \mathbf{v} \cdot \nabla \dot{\boldsymbol{\gamma}} - (\nabla \mathbf{v})^T \cdot \dot{\boldsymbol{\gamma}} - \dot{\boldsymbol{\gamma}} \cdot \nabla \mathbf{v} \tag{5}$$

The kinetic equation of Fredrickson that accounts for the destruction and construction of structure is given by

$$\frac{\mathrm{d}\mu}{\mathrm{d}t} = \frac{\mu}{\lambda}\left(1 - \frac{\mu}{\mu_o}\right) + k\mu\left(1 - \frac{\mu}{\mu_\infty}\right)\boldsymbol{\tau} : \dot{\boldsymbol{\gamma}} \tag{6}$$

where μ is the non-Newtonian viscosity, t is the time of deformation, λ is the relaxation time upon the cessation of steady flow, μ_o and μ_∞ are the viscosities at zero and infinite shear rates respectively, k is a parameter that is related to a critical stress value below which the material exhibits primary creep, $\boldsymbol{\tau}$ is the stress tensor and $\dot{\boldsymbol{\gamma}}$ is the rate of strain tensor. In this model, λ is a structural relaxation time, whereas k is a kinetic constant for structure break down. The elastic modulus G_o is related to these parameters by $G_o = \mu/\lambda$ [40, 41, 42, 43].

Bautista-Manero model was originally proposed for the rheology of worm-like micellar solutions which usually have an upper Newtonian plateau, and show strong signs of shear-thinning. The model, which incorporates shear-thinning, elasticity and thixotropy, can be used to describe the complex rheological behavior of viscoelastic systems that also exhibit thixotropy and rheopexy under shear flow. The model predicts creep behavior, stress relaxation and the presence of thixotropic loops when the sample is subjected to transient stress cycles. The Bautista-Manero model has also been found to fit steady shear, oscillatory and transient measurements of viscoelastic solutions [40, 41, 42, 43].

5.1 Tardy Algorithm

This algorithm is proposed by Philippe Tardy to compute the pressure drop-flow rate relationship for the steady-state flow of a Bautista-Manero fluid in simple capillary network models. The bulk rheology of the fluid and the dimensions of the capillaries making up the network are used as inputs to the models [43]. In the following paragraphs we outline the basic components of this algorithm and the logic behind it. This will be followed by some mathematical and technical details related to the implementation of this algorithm in our non-Newtonian code.

The flow in a single capillary can be described by the following general relation

$$Q = G'\Delta P \tag{7}$$

where Q is the volumetric flow rate, G' is the flow conductance and ΔP is the pressure drop. For a particular capillary and a specific fluid, G' is given by

$$
\begin{aligned}
G' &= G'(\mu) = \text{constant} && \text{Newtonian Fluid} \\
G' &= G'(\mu, \Delta P) && \text{Purely viscous non-Newtonian Fluid} \\
G' &= G'(\mu, \Delta P, t) && \text{Fluid with memory}
\end{aligned} \tag{8}
$$

For a network of capillaries, a set of equations representing the capillaries and satisfying mass conservation should be solved simultaneously to produce a consistent pressure field, as presented in § (4). For Newtonian fluid, a single iteration is needed to solve the pressure field since the conductance is known in advance as the viscosity is constant. For purely viscous non-Newtonian fluid, we start with an initial guess for the viscosity, as it is unknown and pressure-dependent, and solve the pressure field iteratively updating the viscosity after each iteration cycle until convergence is reached. For memory fluids, the dependence on time must be taken into account when solving the pressure field iteratively. Apparently, there is no general strategy to deal with such situation. However, for the steady-state flow of memory fluids a sensible approach is to start with an initial guess for the flow rate and iterate, considering the effect of the local pressure and viscosity variation due to converging-diverging geometry, until convergence is achieved. This approach is adopted by Tardy to find the flow of a Bautista-Manero fluid in a simple capillary network model. In general terms, the Tardy algorithm can be summarized as follows [43]

- For fluids without memory the capillary is unambiguously defined by its radius and length. For fluids with memory, where going from one section to another with different radius is important, the capillary should be modeled with contraction to account for the effect of converging-diverging geometry on the flow. The reason is that the effects of fluid memory take place on going through a radius change, as this change induces a change in shear rate and generation of extensional flow fields with a consequent viscoelastic and thixotropic effects. Examples of the converging-diverging geometries are given in Figure (17).

- Each capillary is discretized in the flow direction and a discretized form of the flow equations is used assuming a prior knowledge of the stress and viscosity at the inlet of the network.

- Starting with an initial guess for the flow rate and using iterative technique, the pressure drop as a function of the flow rate is found for each capillary.

- Finally, the pressure field for the whole network is found iteratively until convergence is achieved. Once the pressure field is found the flow rate through each capillary in the network can be computed and the total flow rate through the network can be determined by summing and averaging the flow through the inlet and outlet capillaries.

A modified version of the Tardy algorithm was implemented in our non-Newtonian code. In the following, we outline the main steps of this algorithm and its implementation.

- From a one-dimensional steady-state Fredrickson equation in which the partial time derivative is written in the form $\frac{\partial}{\partial t} = V\frac{\partial}{\partial x}$, the following equation can be obtained

$$V\frac{\mathrm{d}\mu}{\mathrm{d}x} = \frac{\mu}{\lambda}\left(\frac{\mu_o - \mu}{\mu_o}\right) + k\mu\left(\frac{\mu_\infty - \mu}{\mu_\infty}\right)\tau\dot{\gamma} \qquad (9)$$

In this formulation, the fluid speed V is given by $Q/\pi r^2$ and the average shear rate in the tube with radius r is given by $Q/\pi r^3$.

- By similar argument, another simplified equation can be obtained from the Oldroyd-B model

$$\tau + \frac{V\mu}{G_o}\frac{\mathrm{d}\tau}{\mathrm{d}x} = 2\mu\dot{\gamma} \qquad (10)$$

- The converging-diverging feature of the capillary is implemented in the form of a parabolic profile as outlined in Appendix A.

- Each capillary in the network is discretized into m slices, each with width $\delta x = L/m$ where L is the capillary length.

- From Equation (10), applying the simplified assumption $\frac{\mathrm{d}\tau}{\mathrm{d}x} = \frac{(\tau_2 - \tau_1)}{\delta x}$ where the subscripts 1 and 2 stand for the inlet and outlet of the slice respectively, we obtain an expression for τ_2 in terms of τ_1 and μ_2

$$\tau_2 = \frac{2\mu_2 \dot{\gamma} + \frac{V\mu_2 \tau_1}{G_o \delta x}}{1 + \frac{V\mu_2}{G_o \delta x}} \tag{11}$$

- From Equations (9) and (11), applying $\frac{\mathrm{d}\mu}{\mathrm{d}x} = \frac{(\mu_2 - \mu_1)}{\delta x}$, a third order polynomial in μ_2 is obtained. The coefficients of the four terms of this polynomial are

$$
\begin{aligned}
\mu_2^3 : \quad & -\frac{V}{\lambda \mu_o G_o \delta x} - \frac{2k\dot{\gamma}^2}{\mu_\infty} - \frac{k\dot{\gamma}\tau_1 V}{\mu_\infty G_o \delta x} \\
\mu_2^2 : \quad & -\frac{1}{\lambda \mu_o} - \frac{V^2}{G_o (\delta x)^2} + \frac{V}{\lambda G_o \delta x} + 2k\dot{\gamma}^2 + \frac{k\dot{\gamma}\tau_1 V}{G_o \delta x} \\
\mu_2^1 : \quad & -\frac{V}{\delta x} + \frac{1}{\lambda} + \frac{V^2 \mu_1}{G_o (\delta x)^2} \\
\mu_2^0 : \quad & \frac{V\mu_1}{\delta x}
\end{aligned}
\tag{12}
$$

- The algorithm starts by assuming a Newtonian flow in a network of straight capillaries. Accordingly, the volumetric flow rate Q, and consequently V and $\dot{\gamma}$, for each capillary are obtained.

- Starting from the inlet of the network where the viscosity and the stress are assumed to have known values of μ_o and $R\Delta P/2L$ for each capillary respectively, the computing of the non-Newtonian flow in a converging-diverging geometry takes place in each capillary independently by calculating μ_2 and τ_2 slice by slice, where the values from the previous slice are used for μ_1 and τ_1 of the current slice.

- For the capillaries which are not at the inlet of the network, the initial values of the viscosity and stress at the inlet of the capillary are found by computing the Q-weighted average from all the capillaries that feed into the pore which is at the inlet of the corresponding capillary.

- To find μ_2 of a slice, a bisection numerical method is used. To eliminate possible non-physical roots, the interval for the accepted root is set between zero and $3\mu_o$ with μ_o used in the case of failure. These conditions are logical as long as the slice is reasonably thin and the flow and fluid are physically viable. In the case of a convergence failure, error messages are issued to

inform the user. No failure has been detected during the many runs of this algorithm. Moreover, extensive sample inspection of the μ_2 values has been carried out and proved to be sensible and realistic.

- The value found for the μ_2 is used in conjunction with Equation (11) to find τ_2 which is needed as an input to the next slice.

- Averaging the value of μ_1 and μ_2, the viscosity for the slice is found and used with Poiseuille law to find the pressure drop across the slice.

- The total pressure drop across the whole capillary is computed by summing up the pressure drops across its individual slices. This total is used with Poiseuille law to find the effective viscosity for the capillary as a whole.

- Knowing the effective viscosities for all capillaries of the network, the pressure field is solved iteratively using an algebraic multi-grid solver, and hence the total volumetric flow rate from the network and the apparent viscosity are found.

5.2   Initial Results of the Modified Tardy Algorithm

The modified Tardy algorithm was tested and assessed. Various qualitative aspects were verified and proved to be correct. Some general results and conclusions are outlined below with sample graphs and data for the sand pack and Berea networks using a calculation box with x_l=0.5 and x_u=0.95. We would like to remark that despite our effort to use typical values for the parameters and variables, in some cases we were forced, for demonstration purposes, to use eccentric values to accentuate the features of interest. In Table (1) we present some values for the Bautista-Manero model parameters as obtained from the wormlike micellar system studied by Anderson and co-workers [44] to give an idea of the parameter ranges in real fluids. The system is a solution of a surfactant concentrate [a mixture of the cationic surfactant erucyl bis(hydroxyethyl)methylammonium chloride (EHAC) and 2-propanol in a 3:2 weight ratio] in an aqueous solution of potassium chloride.

5.2.1   Convergence-Divergence

A dilatant effect due to the converging-diverging feature has been detected relative to a network of straight capillaries. The viscosity increase is a natural viscoelastic

Table 1: Some values of the wormlike micellar system studied by Anderson and co-workers [44] which is a solution of surfactant concentrate (a mixture of EHAC and 2-propanol) in an aqueous solution of potassium chloride.

Parameter	Value
G_o (Pa)	1 - 10
μ_o (Pa.s)	115 - 125
μ_∞ (Pa.s)	0.00125 - 0.00135
λ (s)	1 - 30
k (Pa^{-1})	10^{-3} - 10^{-6}

response to the radius tightening at the middle. As the corrugation feature of the tubes is exacerbated by narrowing the radius at the middle, the viscoelastic dilatant behavior is intensified. The natural explanation is that the increase in apparent viscosity should be proportionate to the magnitude of tightening. This feature is presented in Figures (1) and (2) for the sand pack and Berea networks respectively on a log-log scale.

5.2.2 Diverging-Converging

The investigation of the effect of diverging-converging geometry by expanding the radius of the capillaries at the middle revealed a thinning effect relative to the straight and converging-diverging geometries, as seen in Figures (3) and (4) for the sand pack and Berea networks respectively on a log-log scale. This is due to viscoelastic response in the opposite sense to that of converging-diverging by enlarging the radius at the middle.

5.2.3 Number of Slices

As the number of slices of the capillaries increases, the algorithm converges to a stable and constant solution within acceptable numerical errors. This indicates that the numerical aspects of the algorithm are functioning correctly because the effect of discretization errors is expected to diminish by increasing the number of slices and hence decreasing their width. A sample graph of apparent viscosity versus number of slices for a typical data point is presented in Figure (5) for the sand pack and in Figure (6) for Berea.
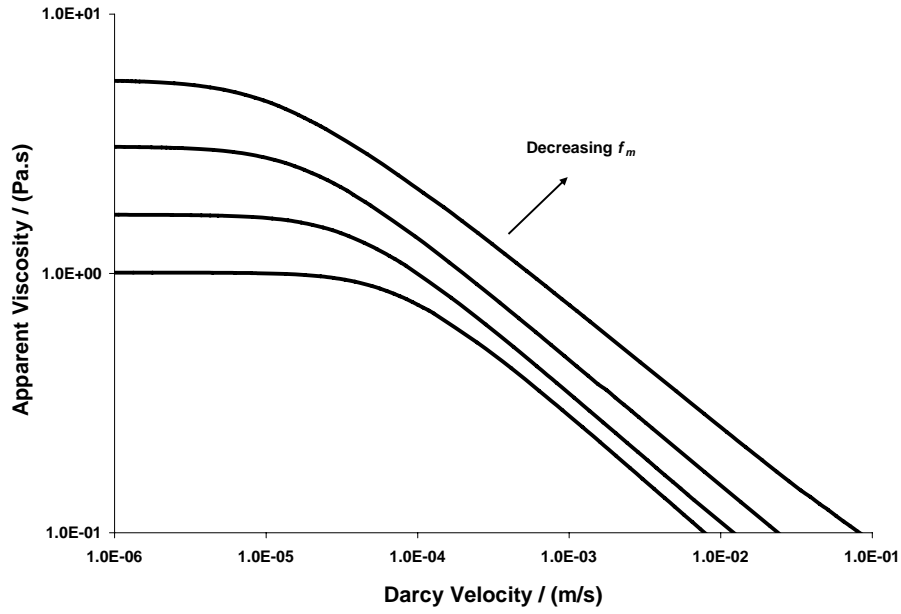
Figure 1: The Tardy algorithm sand pack results for G_o=0.1 Pa, μ_∞=0.001 Pa.s, μ_o=1.0 Pa.s, λ=1.0 s, k=10^{-5} Pa^{-1}, f_e=1.0, m=10 slices, with varying f_m (1.0, 0.8, 0.6 and 0.4).
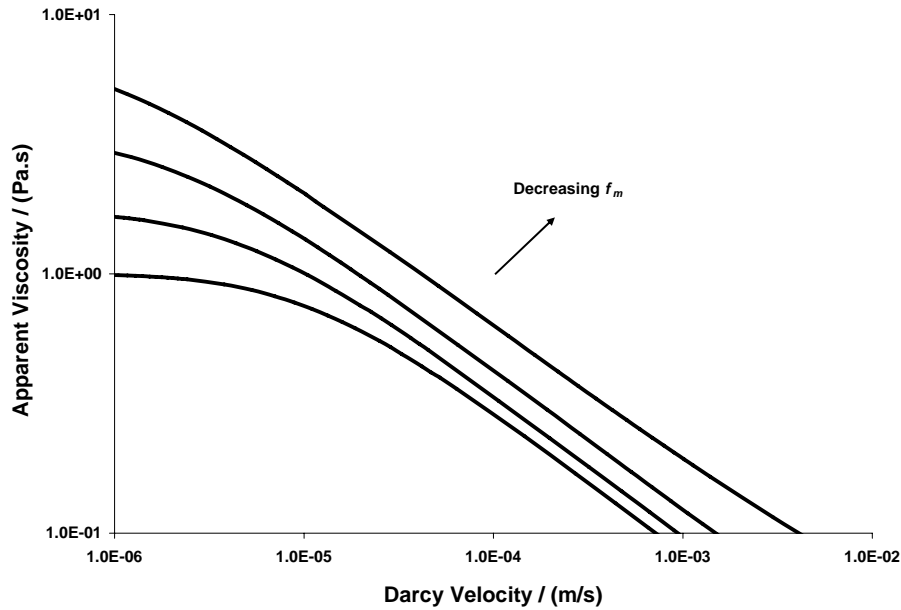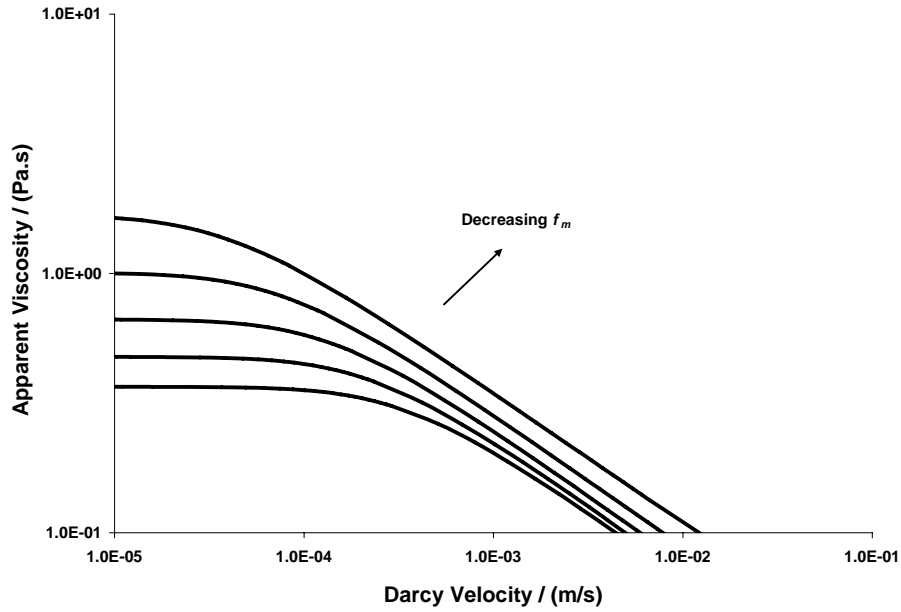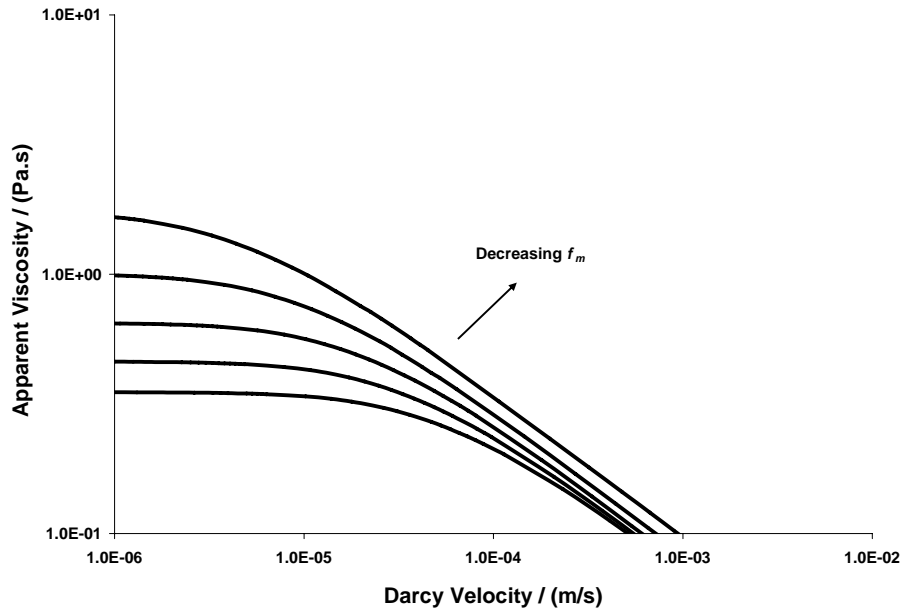

Figure 2: The Tardy algorithm Berea results for G_o=0.1 Pa, μ_∞=0.001 Pa.s, μ_o=1.0 Pa.s, λ=1.0 s, k=10^{-5} Pa^{-1}, f_e=1.0, m=10 slices, with varying f_m (1.0, 0.8, 0.6 and 0.4).

Figure 3: The Tardy algorithm sand pack results for G_o=0.1 Pa, μ_∞=0.001 Pa.s, μ_o=1.0 Pa.s, λ=1.0 s, k=10^{-5} Pa^{-1}, f_e=1.0, m=10 slices, with varying f_m (0.8, 1.0, 1.2, 1.4 and 1.6).

Figure 4: The Tardy algorithm Berea results for G_o=0.1 Pa, μ_∞=0.001 Pa.s, μ_o=1.0 Pa.s, λ=1.0 s, k=10^{-5} Pa^{-1}, f_e=1.0, m=10 slices, with varying f_m (0.8, 1.0, 1.2, 1.4 and 1.6).

5.2.4 Boger Fluid

A Boger fluid behavior was observed when setting $\mu_o = \mu_\infty$. However, the apparent viscosity increased as the converging-diverging feature is intensified. This feature is
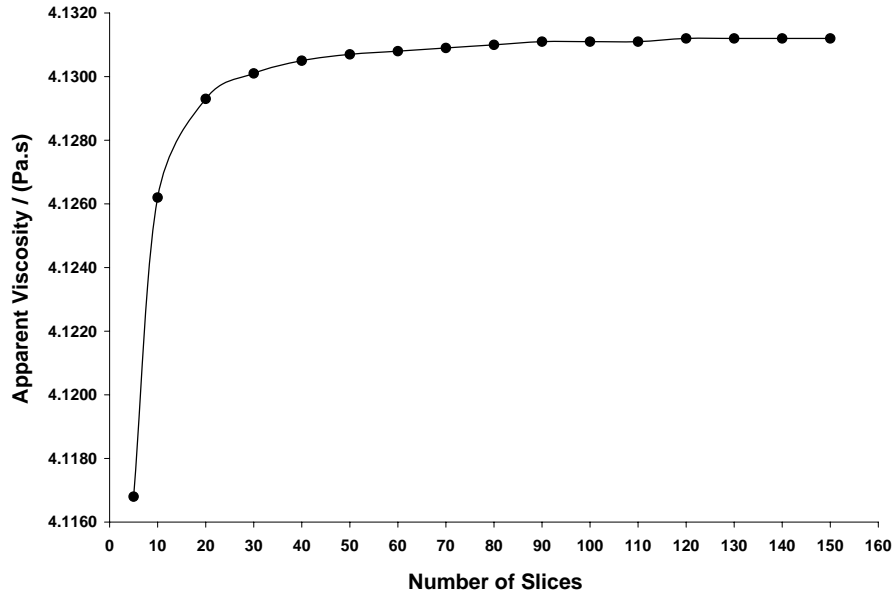
Figure 5: The Tardy algorithm sand pack results for G_o=1.0 Pa, μ_∞=0.001 Pa.s, μ_o=1.0 Pa.s, λ=1.0 s, k=10^{-5} Pa^{-1}, f_e=1.0, f_m=0.5, with varying number of slices for a typical data point (ΔP=100 Pa).
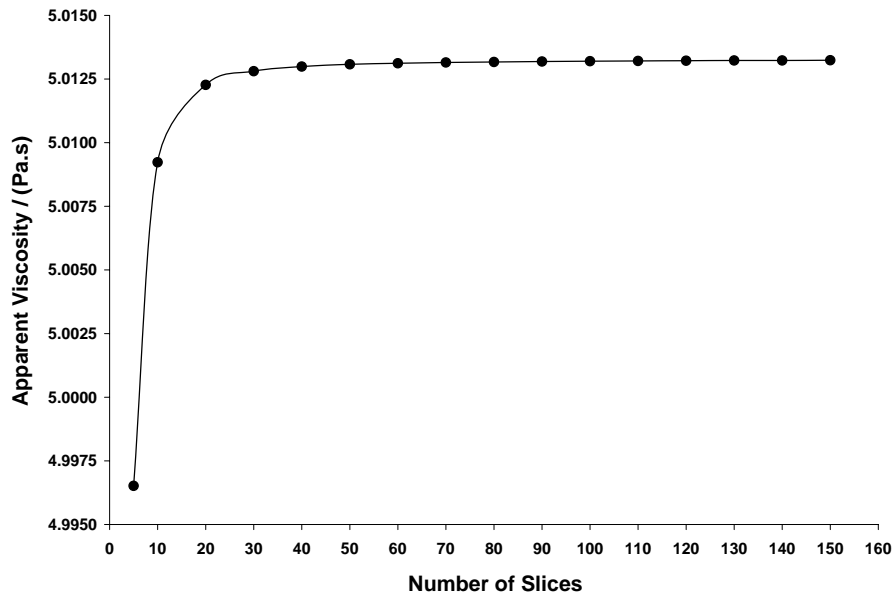

Figure 6: The Tardy algorithm Berea results for G_o=1.0 Pa, μ_∞=0.001 Pa.s, μ_o=1.0 Pa.s, λ=1.0 s, k=10^{-5} Pa^{-1}, f_e=1.0, f_m=0.5, with varying number of slices for a typical data point (ΔP=200 Pa).

demonstrated in Figure (7) for the sand pack and in Figure (8) for Berea on a log-log scale. Since Boger fluid is a limiting and obvious case, this behavior indicates

that the model, as implemented, is well-behaved. The viscosity increase is a natural viscoelastic response to the radius tightening at the middle, as discussed earlier.

5.2.5 Elastic Modulus

The effect of the elastic modulus G_o was investigated for shear-thinning fluids, i.e. $\mu_o > \mu_\infty$, by varying this parameter over several orders of magnitude while holding the others constant. It was observed that by increasing G_o, the high-shear apparent viscosities were increased while the low-shear viscosities remained constant and have not been affected. However, the increase at high-shear rates has almost reached a saturation point where beyond some limit the apparent viscosities converged to certain values despite a large increase in G_o. A sample of the results for this investigation is presented in Figure (9) for the sand pack and in Figure (10) for Berea on a log-log scale. The stability at low-shear rates is to be expected because at low flow rate regimes near the lower Newtonian plateau the non-Newtonian effects due to elastic modulus are negligible. As the elastic modulus increases, an increase in apparent viscosity due to elastic effects contributed by elastic modulus occurs. Eventually, a saturation will be reached when the contribution of this factor is controlled by other dominant factors and mechanisms from the porous medium and flow regime.

5.2.6 Shear-Thickening

A slight shear-thickening effect was observed when setting $\mu_o < \mu_\infty$ while holding the other parameters constant. The effect of increasing G_o on the apparent viscosities at high-shear rates was similar to the effect observed for the shear-thinning fluids though it was at a smaller scale. However, the low-shear viscosities are not affected, as in the case of shear-thinning fluids. A convergence for the apparent viscosities at high-shear rates for large values of G_o was also observed as for shear-thinning. A sample of the results obtained in this investigation is presented in Figures (11) and (12) for the sand pack and Berea networks respectively on a log-log scale. It should be remarked that as the Bautista-Manero is originally a shear-thinning model, it should not be expected to fully-predict shear-thickening phenomenon. However, the observed behavior is a good sign for our model because as we push the algorithm beyond its limit, the results are still qualitatively reasonable.
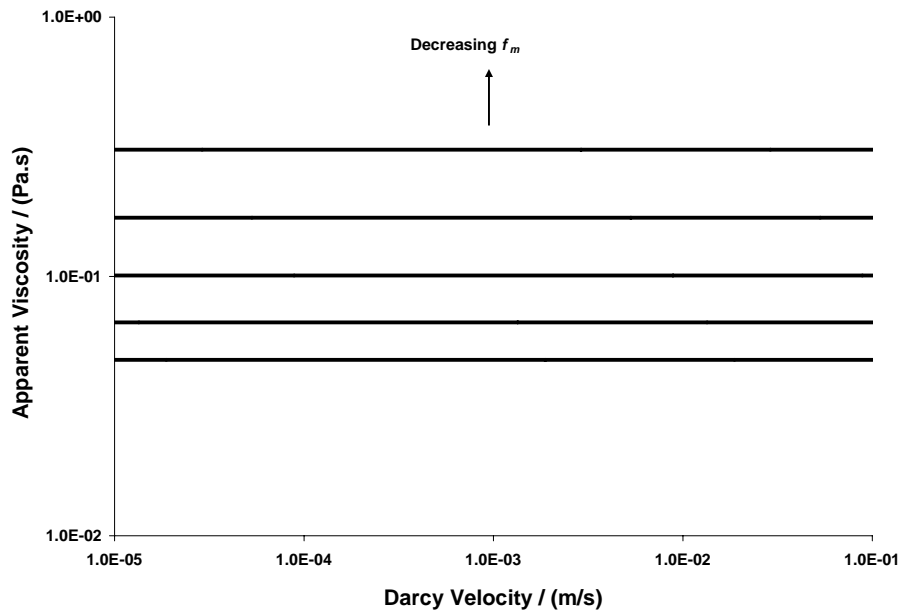
Figure 7: The Tardy algorithm sand pack results for G_o=1.0 Pa, μ_∞=μ_o=0.1 Pa.s, λ=1.0 s, k=10^{-5} Pa^{-1}, f_e=1.0, m=10 slices, with varying f_m (0.6, 0.8, 1.0, 1.2 and 1.4).
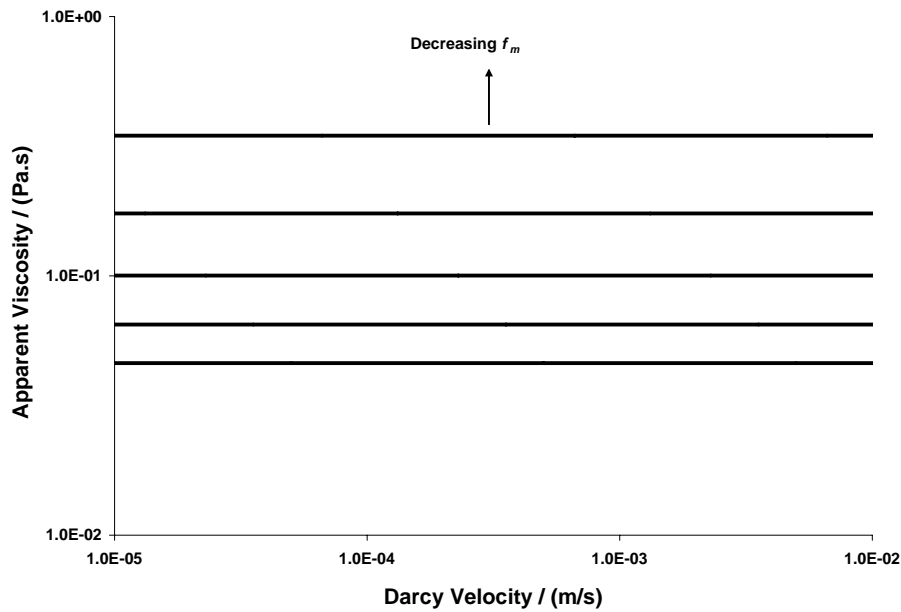

Figure 8: The Tardy algorithm Berea results for G_o=1.0 Pa, μ_∞=μ_o=0.1 Pa.s, λ=1.0 s, k=10^{-5} Pa^{-1}, f_e=1.0, m=10 slices, with varying f_m (0.6, 0.8, 1.0, 1.2 and 1.4).
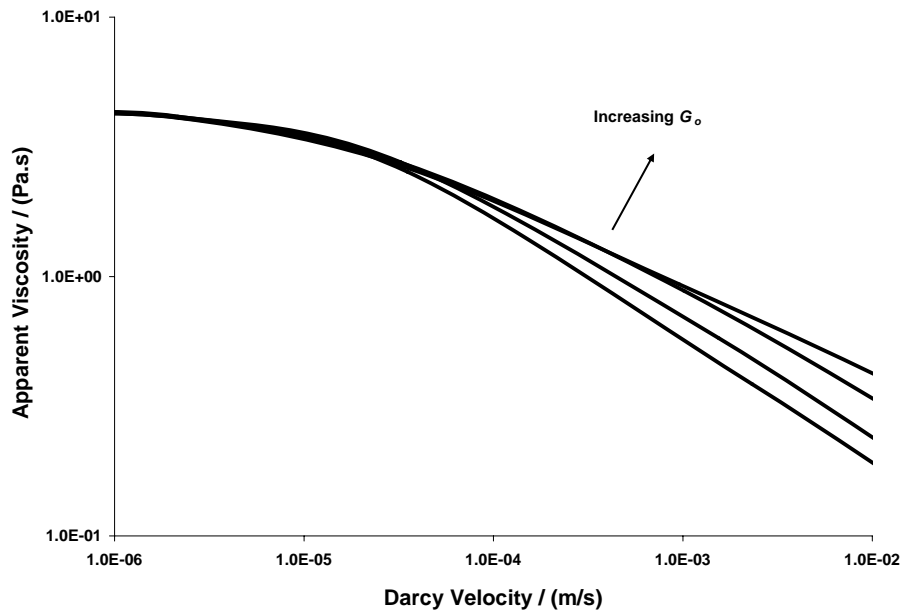
Figure 9: The Tardy algorithm sand pack results for μ_∞=0.001 Pa.s, μ_o=1.0 Pa.s, λ=1.0 s, k=10^{-5} Pa^{-1}, f_e=1.0, f_m=0.5, m=10 slices, with varying G_o (0.1, 1.0, 10 and 100 Pa).
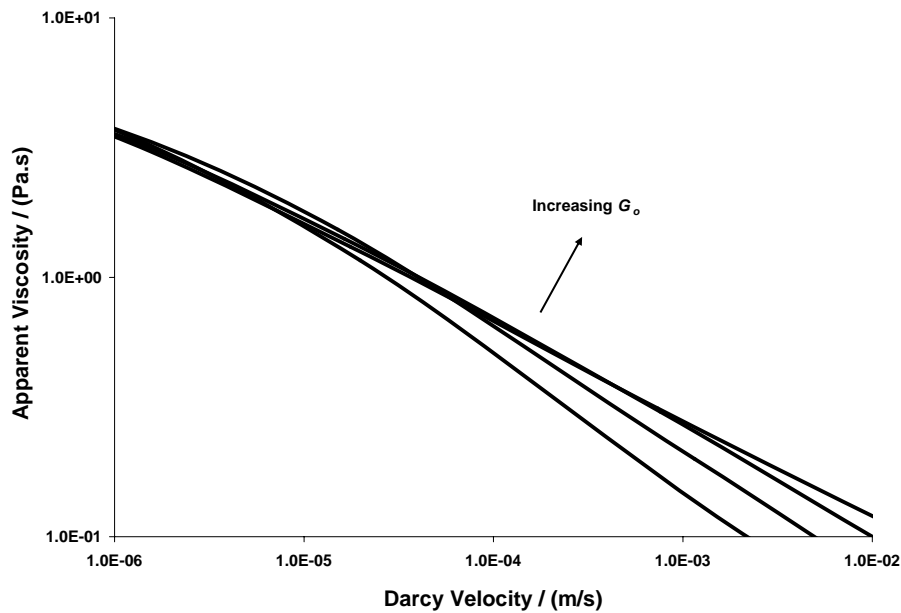

Figure 10: The Tardy algorithm Berea results for μ_∞=0.001 Pa.s, μ_o=1.0 Pa.s, λ=1.0 s, k=10^{-5} Pa^{-1}, f_e=1.0, f_m=0.5, m=10 slices, with varying G_o (0.1, 1.0, 10 and 100 Pa).

5.2.7 Relaxation Time

The effect of the structural relaxation time λ was investigated for shear-thinning fluids by varying this parameter over several orders of magnitude while holding
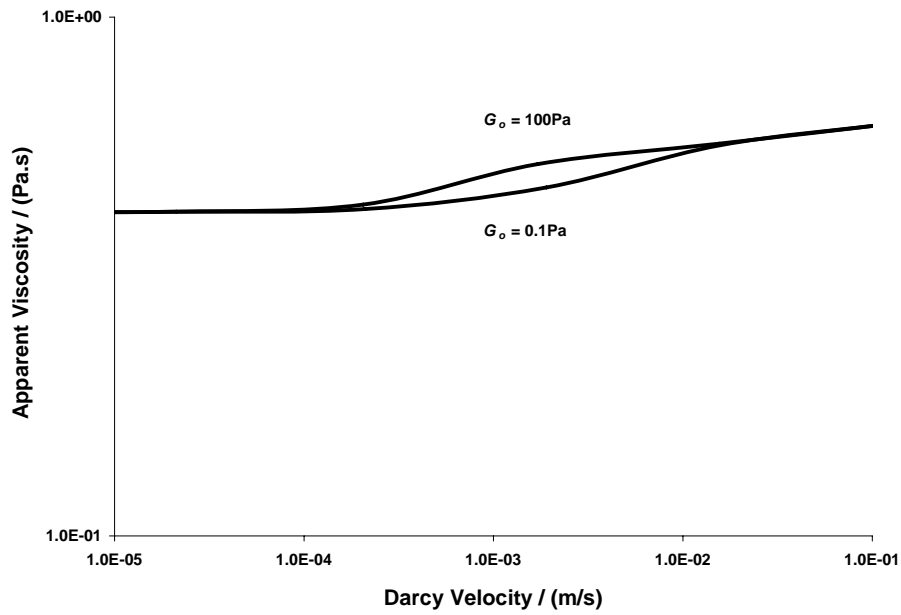
Figure 11: The Tardy algorithm sand pack results for μ_∞=10.0 Pa.s, μ_o=0.1 Pa.s, λ=1.0 s, k=10^{-4} Pa^{-1}, f_e=1.0, f_m=0.5, m=10 slices, with varying G_o (0.1 and 100 Pa).
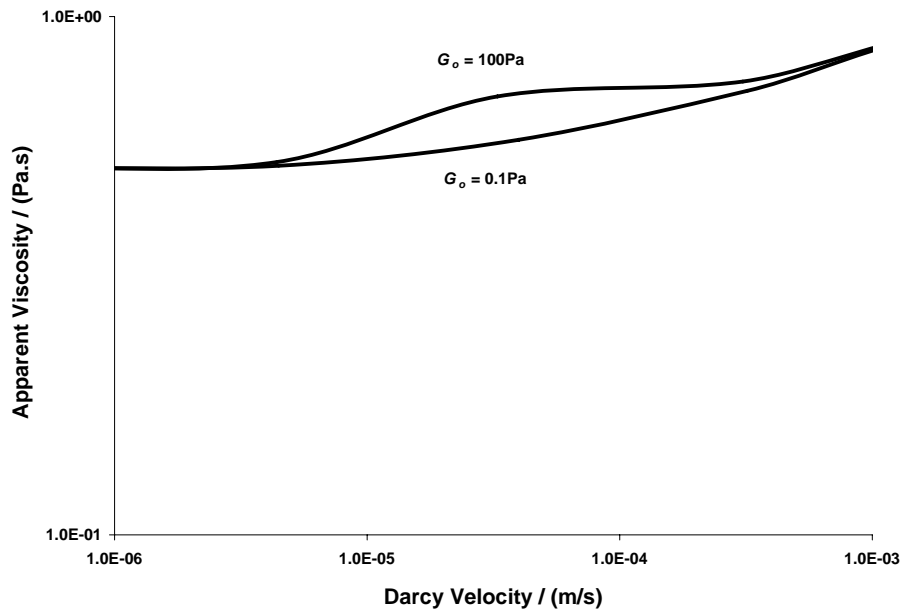

Figure 12: The Tardy algorithm Berea results for μ_∞=10.0 Pa.s, μ_o=0.1 Pa.s, λ=1.0 s, k=10^{-4} Pa^{-1}, f_e=1.0, f_m=0.5, m=10 slices, with varying G_o (0.1 and 100 Pa).

the others constant. It was observed that by increasing the structural relaxation time, the apparent viscosities were steadily decreased. However, the decrease at

high-shear rates has almost reached a saturation point where beyond some limit the apparent viscosities converged to certain values despite a large increase in λ. A sample of the results is given in Figure (13) for the sand pack and Figure (14) for Berea on a log-log scale. The effects of relaxation time are expected to ease as the relaxation time increases beyond a limit such that the effect of interaction with capillary constriction is negligible. Despite the fact that this feature requires extensive investigation for quantitative confirmation, the observed behavior seems qualitatively reasonable considering the flow regimes and the size of relaxation times of the sample results.

5.2.8 Kinetic Parameter

The effect of the kinetic parameter for structure break down k was investigated for shear-thinning fluids by varying this parameter over several orders of magnitude while holding the others constant. It was observed that by increasing the kinetic parameter, the apparent viscosities generally decreased. However, in some cases the low-shear viscosities has not been substantially affected. A sample of the results is given in Figures (15) and (16) for the sand pack and Berea networks respectively on a log-log scale. The decrease in apparent viscosity on increasing the kinetic parameter is a natural response as the parameter quantifies structure break down and hence reflects thinning mechanisms. It is a general trend that the low flow rate regimes near the lower Newtonian plateau are usually less influenced by non-Newtonian effects. It will therefore be natural that the low-shear viscosities in some cases experienced minor changes.
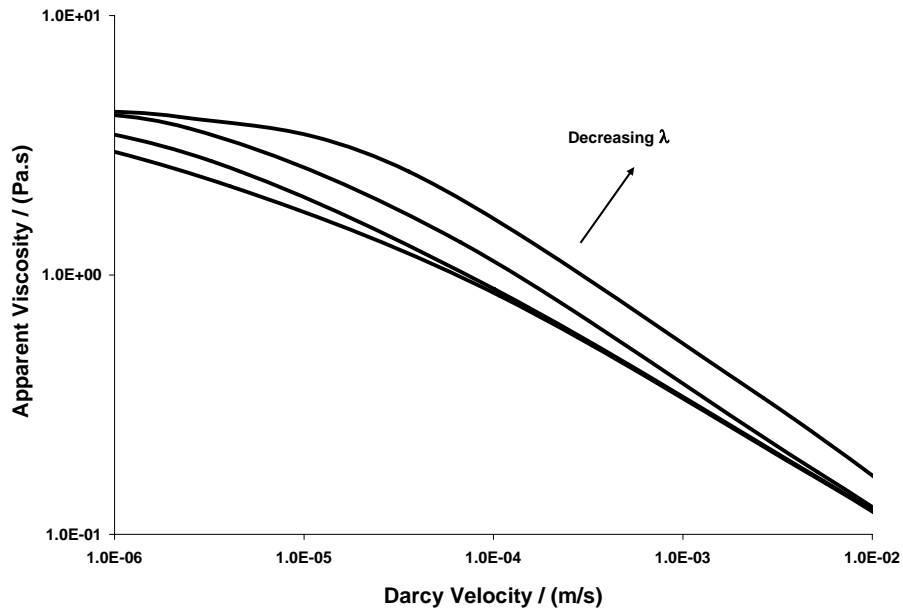
Figure 13: The Tardy algorithm sand pack results for G_o=1.0 Pa, μ_∞=0.001 Pa.s, μ_o=1.0 Pa.s, k=10^{-5} Pa^{-1}, f_e=1.0, f_m=0.5, m=10 slices, with varying λ (0.1, 1.0, 10, and 100 s).
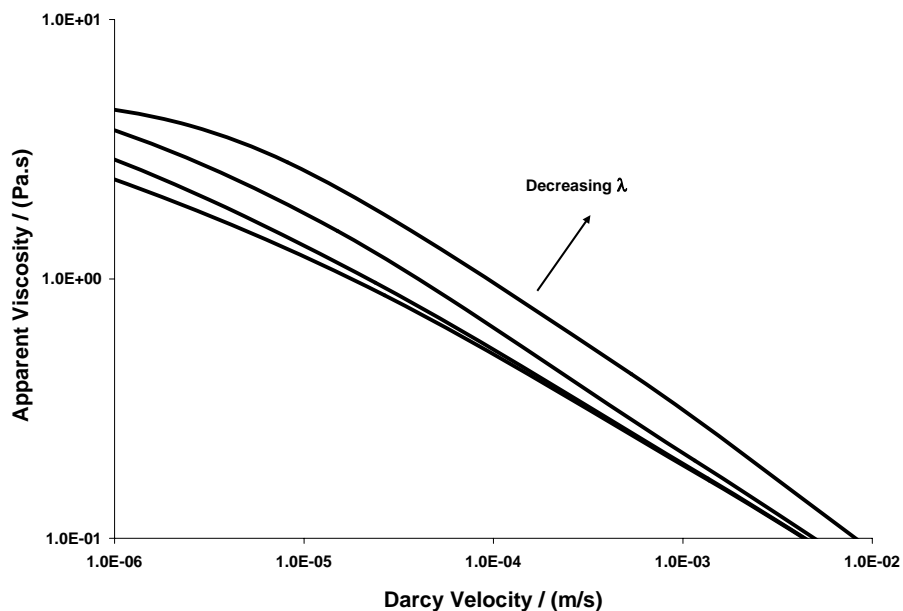

Figure 14: The Tardy algorithm Berea results for G_o=1.0 Pa, μ_∞=0.001 Pa.s, μ_o=1.0 Pa.s, k=10^{-5} Pa^{-1}, f_e=1.0, f_m=0.5, m=10 slices, with varying λ (0.1, 1.0, 10, and 100 s).
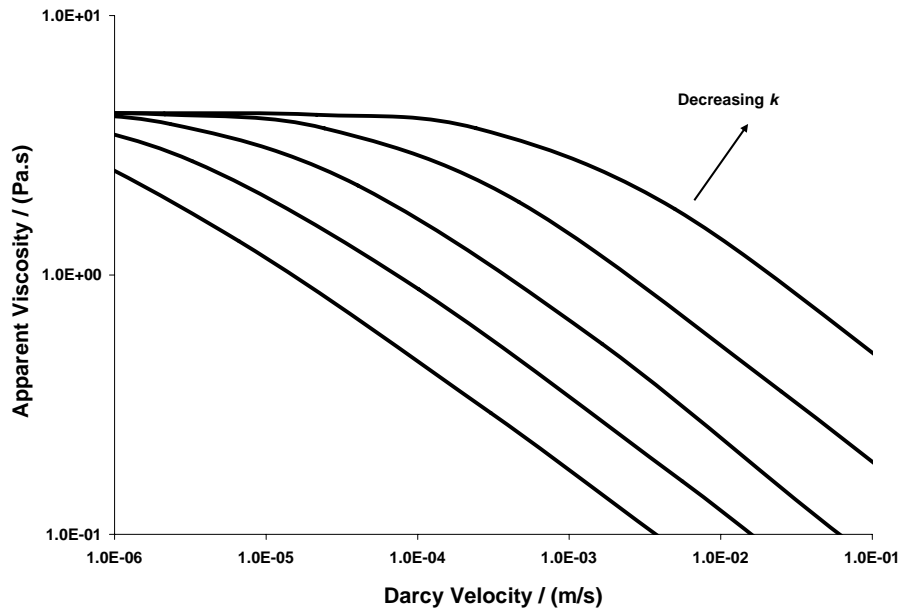
Figure 15: The Tardy algorithm sand pack results for G_o=1.0 Pa, μ_∞=0.001 Pa.s, μ_o=1.0 Pa.s, λ=10 s, f_e=1.0, f_m=0.5, m=10 slices, with varying k (10^{-3}, 10^{-4}, 10^{-5}, 10^{-6} and 10^{-7} Pa^{-1}).
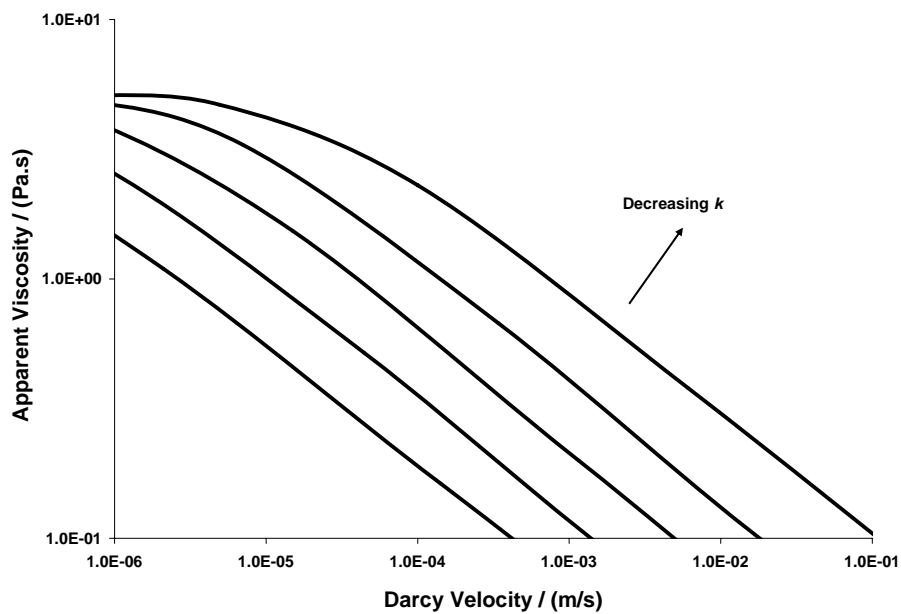

Figure 16: The Tardy algorithm Berea results for G_o=1.0 Pa, μ_∞=0.001 Pa.s, μ_o=1.0 Pa.s, λ=1.0 s, f_e=1.0, f_m=0.5, m=10 slices, with varying k (10^{-3}, 10^{-4}, 10^{-5}, 10^{-6} and 10^{-7} Pa^{-1}).

6 Conclusions

A non-Newtonian flow simulation code based on pore-scale network modeling has been extended to account for viscoelastic and thixotropic behavior using a Bautista-Manero fluid model. The basis of the implementation is a numerical algorithm originally suggested by Philippe Tardy. A modified version of this algorithm was used to investigate the effect of converging-diverging geometry on the steady-state flow. The implementation of this model has been examined and assessed using a sand pack and a Berea networks. The generic behavior indicates qualitatively correct trends. A conclusion was reached that the current implementation is a proper basis for investigating the steady-state viscoelastic effects and some thixotropic effects due to converging-diverging geometries in porous media. This implementation can be used as a suitable foundation for further development. The future work can include elaborating the modified Tardy algorithm and thoroughly investigating its viscoelastic and thixotropic predictions in quantitative terms. The code (called Non-Newtonian Code 2) with complete documentation and the networks can be obtained from this URL: http://www3.imperial.ac.uk/earthscienceandengineerinresearch/perm/porescalemodellinsoftware/non-newtonian%20code.

Acknowledgements

Nomenclature

$\dot{\gamma}$ strain rate (s^{-1})

$\dot{\boldsymbol{\gamma}}$ rate-of-strain tensor

λ structural relaxation time in Fredrickson model (s)

λ_1 relaxation time (s)

λ_2 retardation time (s)

μ viscosity (Pa.s)

μ_o zero-shear viscosity (Pa.s)

μ_∞ infinite-shear viscosity (Pa.s)

τ stress (Pa)

$\boldsymbol{\tau}$ stress tensor

f_e scale factor for the entry of corrugated tube (—)

f_m scale factor for the middle of corrugated tube (—)

G geometric conductance (m^4)

G' flow conductance ($m^3.Pa^{-1}.s^{-1}$)

G_o elastic modulus (Pa)

k parameter in Fredrickson model (Pa^{-1})

L tube length (m)

P pressure (Pa)

ΔP pressure drop (Pa)

Q volumetric flow rate ($m^3.s^{-1}$)

r radius (m)

R tube radius (m)

R_{eq} equivalent radius (m)

R_{max} maximum radius of corrugated capillary

R_{min} minimum radius of corrugated capillary

t time (s)

$\mathbf{v}$ fluid velocity vector

$\nabla\mathbf{v}$ fluid velocity gradient tensor

V	fluid speed (m.s^{-1})
δx	small change in x (m)
$\overset{\triangledown}{\cdot}$	upper convected time derivative
$(\cdot)^T$	matrix transpose
x_l	network lower boundary in the non-Newtonian code
x_u	network upper boundary in the non-Newtonian code

Note: units, when relevant, are given in the SI system. Vectors and tensors are marked with boldface. Some symbols may rely on the context for unambiguous identification.

References

[1] A.H.P. Skelland. *Non-Newtonian Flow and Heat Transfer.* John Wiley and Sons Inc., 1967. 6, 15

[2] R.P. Chhabra; J.F. Richardson. *Non-Newtonian Flow in the Process Industries.* Butterworth Heinemann Publishers, 1999. 6

[3] H.A. Barnes; J.E Hutton; K. Walters. *An introduction to rheology.* Elsevier, 1993. 6, 8, 10, 11

[4] R.G. Larson. *Constitutive Equations for Polymer Melts and Solutions.* Butterworth Publishers, 1988. 7, 8

[5] R.G. Larson. *The Structure and Rheology of Complex Fluids.* Oxford University Press, 1999. 7, 9, 11

[6] M.A. Hulsen. *A discontinuous Galerkin method with splitting applied to viscoelastic flow.* Faculty of Mechanical Engineering and Marine Technology, Delft University of Technology, 1986. 7

[7] R. Keunings. Micro-macro methods for the multi-scale simulation of viscoelastic flow using molecular models of kinetic theory. *Rheology Reviews*, pages 67–98, 2004. 7, 13

[8] R.G. Owens; T.N. Phillips. *Computational Rheology.* Imperial College Press, 2002. 7, 8

[9] M.M. Denn. Issues in viscoelastic fluid mechanics. *Annual Review of Fluid Mechanics*, 22:13–34, 1990. 7

[10] J.A. Deiber. *Modeling the flow of Newtonian and viscoelastic fluids through porous media.* PhD thesis, Princeton University, 1978. 7, 8, 9, 10, 11, 12

[11] D.V. Boger. Viscoelastic flows through contractions. *Annual Review of Fluid Mechanics*, 19:157–182, 1987. 7, 8

[12] R.B. Bird; R.C. Armstrong; O. Hassager. *Dynamics of Polymeric Liquids*, volume 1. John Wily & Sons, second edition, 1987. 8, 13, 17

[13] P. Wapperom. *Nonisothermal flows of viscoelastic fluids Thermodynamics, analysis and numerical simulation.* PhD thesis, Delft University of Technology, 1996. 8, 11

[14] E.H. Wissler. Viscoelastic effects in the flow of non-Newtonian fluids through a porous medium. *Industrial & Engineering Chemistry Fundamentals*, 10(3):411–417, 1971. 9

[15] R.P. Chhabra; J. Comiti; I. Machač. Flow of non-Newtonian fluids in fixed and fluidised beds. *Chemical Engineering Science*, 56(1):1–27, 2001. 9, 10, 12

[16] R.J. Marshall; A.B. Metzner. Flow of viscoelastic fluids through porous media. *Industrial & Engineering Chemistry Fundamentals*, 6(3):393–400, 1967. 9, 11

[17] D.L. Dauben; D.E. Menzie. Flow of polymer solutions through porous media. *Journal of Petroleum Technology, SPE 1688-PA*, pages 1065–1073, 1967. 9

[18] J.R.A. Pearson; P.M.J. Tardy. Models for flow of non-Newtonian and complex fluids through porous media. *Journal of Non-Newtonian Fluid Mechanics*, 102:447–473, 2002. 9

[19] J.P. Plog; W.M. Kulicke. Flow behaviour of dilute hydrocolloid solutions through porous media. Influence of molecular weight, concentration and solvent. *Institute of Technical and Macromolecular Chemistry, University of Hamburg.* 9, 10

[20] P.R.S. Mendes; M.F. Naccache. A constitutive equation for extensional-thickening fluids flowing through porous media. *Proceedings of 2002 ASME International Mechanical Engineering Congress & Exposition, November 17-22, New Orleans, Louisiana, USA*, 2002. 9

[21] N. Phan-Thien; M.M.K. Khan. Flow of an Oldroyd-type fluid through a sinusoidally corrugated tube. *Journal of Non-Newtonian Fluid Mechanics*, 24:203–220, 1987. 10

[22] J.A. Deiber; W.R. Schowalter. Modeling the flow of viscoelastic fluids through porous media. *AIChE Journal*, 27(6):912–920, 1981. 10, 11

[23] S. Pilitsis; A.N. Beris. Calculations of steady-state viscoelastic flow in an undulating tube. *Journal of Non-Newtonian Fluid Mechanics*, 31(3):231–287, 1989. 10, 11, 12

[24] K.S. Sorbie. *Polymer-Improved Oil Recovery.* Blakie and Son Ltd, 1991. 10

[25] P.J. Carreau; D. De Kee; R.P. Chhabra. *Rheology of Polymeric Systems.* Hanser Publishers, 1997. 10, 13

[26] K.F.J. Denys. *Flow of polymer solutions through porous media*. PhD thesis, Delft University of Technology, 2003. 11, 12

[27] F. Durst; R. Haas; W. Interthal. The nature of flows through porous media. *Journal of Non-Newtonian Fluid Mechanics*, 22(2):169–189, 1987. 11

[28] A. Souvaliotis; A.N. Beris. Applications of domain decomposition spectral collocation methods in viscoelastic flows through model porous media. *Journal of Rheology*, 36(7):1417–1453, 1992. 11

[29] K.K. Talwar; B. Khomami. Application of higher order finite element methods to viscoelastic flow in porous media. *Journal of Rheology*, 36(7):1377–1416, 1992. 12

[30] A.K. Podolsak; C. Tiu; T.N. Fang. Flow of non-Newtonian fluids through tubes with abrupt expansions and contractions (square wave tubes). *Journal of Non-Newtonian Fluid Mechanics*, 71(1):25–39, 1997. 12

[31] M.A. Hulsen. *A numerical method for solving steady 2D and axisymmetrical viscoelastic flow problems with an application to inertia effects in contraction flows*. Faculty of Mechanical Engineering, Delft University of Technology, 1990. 13

[32] M.A. Hulsen. *Analysis of the equations for viscoelastic flow: Type, boundary conditions, and discontinuities*. Faculty of Mechanical Engineering, Delft University of Technology, 1986. 13

[33] R. Keunings. Finite element methods for integral viscoelastic fluids. *Rheology Reviews*, pages 167–195, 2003. 13

[34] M.J. Blunt; M.D. Jackson; M. Piri; P.H. Valvatne. Detailed physics, predictive capabilities and macroscopic consequences for pore-network models of multiphase flow. *Advances in Water Resources*, 25:1069–1089, 2002. 14

[35] M.J. Blunt. Flow in porous media - pore-network models and multiphase flow. *Colloid and Interface Science*, 6(3):197–207, 2001. 14

[36] P.E. Øren; S. Bakke; O.J. Amtzen. Extending predictive capabilities to network models. *SPE Annual Technical Conference and Exhibition, San Antonio, Texas*, (SPE 38880), 1997. 14

[37] P.E. Øren; S. Bakke. Reconstruction of berea sandstone and pore-scale modelling of wettability effects. *Journal of Petroleum Science and Engineering*, 39:177–199, 2003. 14

[38] T. Sochi; M.J. Blunt. Pore-scale network modeling of Ellis and Herschel-Bulkley fluids. *Journal of Petroleum Science and Engineering*, 60(2):105–124, 2008. 15

[39] J.W. Ruge; K. Stüben. *Multigrid Methods: Chapter 4 (Algebraic Multigrid), Frontiers in Applied Mathematics*. SIAM, 1987. 15

[40] F. Bautista; J.M. de Santos; J.E. Puig; O. Manero. Understanding thixotropic and antithixotropic behavior of viscoelastic micellar solutions and liquid crystalline dispersions. I. The model. *Journal of Non-Newtonian Fluid Mechanics*, 80(2):93–113, 1999. 18

[41] F. Bautista; J.F.A. Soltero; J.H. Pérez-López; J.E. Puig; O. Manero. On the shear banding flow of elongated micellar solutions. *Journal of Non-Newtonian Fluid Mechanics*, 94(1):57–66, 2000. 18

[42] O. Manero; F. Bautista; J.F.A. Soltero; J.E. Puig. Dynamics of worm-like micelles: the Cox-Merz rule. *Journal of Non-Newtonian Fluid Mechanics*, 106(1):1–15, 2002. 18

[43] P. Tardy; V.J. Anderson. Current modelling of flow through porous media. *Private communication*, 2005. 18, 19

[44] V.J. Anderson; J.R.A. Pearson; J.D. Sherwood. Oscillation superimposed on steady shearing: Measurements and predictions for wormlike micellar solutions. *Journal of Rheology*, 50(5):771–796, 2006. 22, 23

Appendix A: Converging-Diverging Geometry and Tube Discretization

There are many simplified converging-diverging geometries for corrugated capillaries which can be used to model the flow of viscoelastic fluids in porous media; some suggestions are presented in Figure (17). In this study we adopted the paraboloid and hence developed simple formulae to find the radius as a function of the distance along the tube axis, assuming cylindrical coordinate system, as shown in Figure (18).

For the paraboloid depicted in Figure (18), we have

$$r(z) = az^2 + bz + c \tag{13}$$

Since

$$r(-L/2) = r(L/2) = R_{max} \qquad \& \qquad r(0) = R_{min} \tag{14}$$

the paraboloid is uniquely identified by these three points. On substituting and solving these equations simultaneously, we obtain

$$a = \left(\frac{2}{L}\right)^2 (R_{max} - R_{min}) \qquad b = 0 \qquad \& \qquad c = R_{min} \tag{15}$$

that is

$$r(z) = \left(\frac{2}{L}\right)^2 (R_{max} - R_{min})z^2 + R_{min} \tag{16}$$

In the modified Tardy algorithm for steady-state viscoelastic flow as implemented in our non-Newtonian code, when a capillary is discretized into m slices the radius $r(z)$ is sampled at m z-points given by

$$z = -\frac{L}{2} + k\frac{L}{m} \qquad (k = 1, ..., m) \tag{17}$$

More complex polynomial and sinusoidal converging-diverging profiles can also be modeled using this approach.
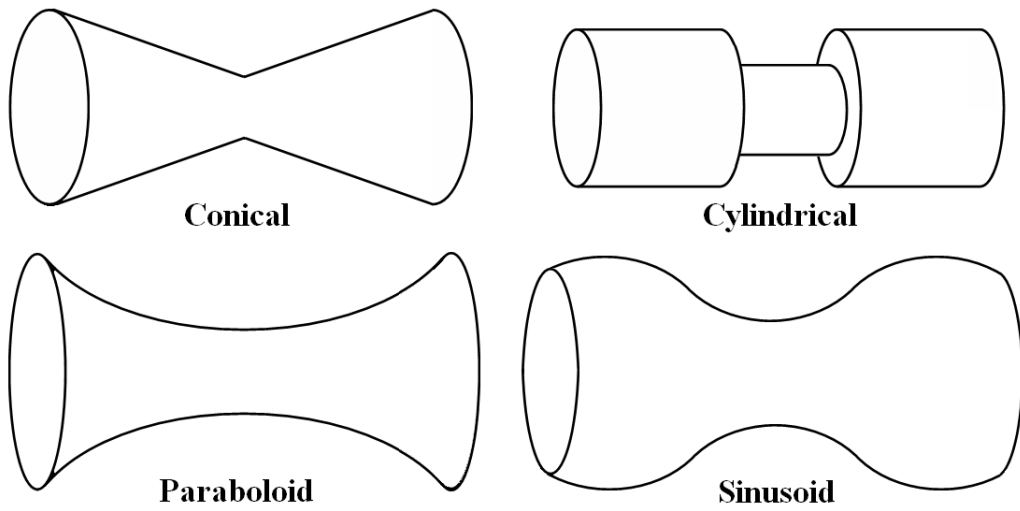
Figure 17: Examples of corrugated capillaries which can be used to model converging-diverging geometry in porous media.
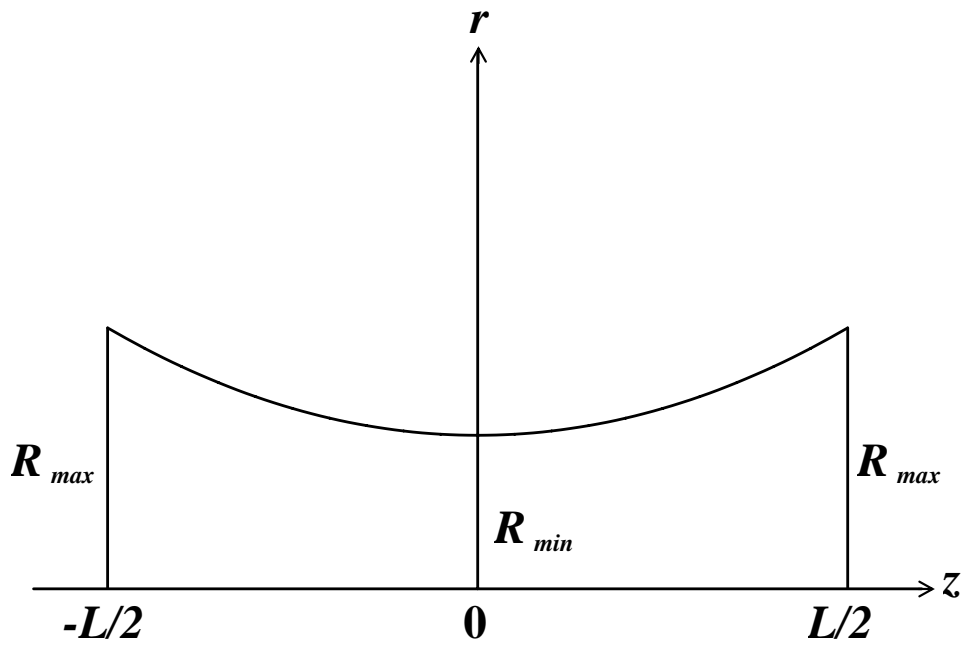

Figure 18: Radius variation in the axial direction for a corrugated paraboloid capillary using a cylindrical coordinate system.

43